Investigation of the Electric Field in TiO_2/FTO Junctions Used in Dye-Sensitized Solar Cells by Photocurrent Transients

Sven Rühle*,† and Thomas Dittrich‡,§

Department of Materials and Interfaces, Weizmann Institute of Science, Rehovot 76100, Israel, and Hahn-Meitner-Institut, Glienicker Strasse 100, 14109 Berlin, Germany

Received: August 22, 2004; In Final Form: February 21, 2005

We have investigated the electrostatic potential distribution in compact and nanoporous TiO_2 films, deposited on conducting F-doped SnO_2 substrate (FTO), which are used in dye-sensitized solar cells. The TiO_2 films were immersed into aqueous electrolyte and excited from the FTO side by light pulses of a N_2 laser while the current response was measured as a function of time. The measurements were carried out as a function of the pH value of the electrolyte and at different electrostatic potentials. For compact TiO_2 films, the sign of the transient current at short response times changed when the applied electrostatic potential or the pH value was decreased. This was not observed for mesoporous TiO_2 films directly deposited onto the FTO substrate without a compact TiO_2 layer. We interpret the results in terms of a macroscopic electric field across the compact layer which is changed by the applied potential or the pH of the electrolyte. In contrast, measurements on mesoporous TiO_2 films indicate that the contact region is mainly field-free, and we explain our results by a very sharp electrostatic potential drop within the first layer of particles at the TiO_2/FTO interface.

Introduction

The electrostatic potential distribution at the F-doped SnO_2 substrate (FTO)/TiO_2 interface plays an important role for a better understanding of the working principle of dye-sensitized solar cells (DSSCs) and of nanocomposite solar cells with an extremely thin absorber (so-called ETA cells). The working principle of DSSCs and solid-state equivalents is still under debate. Especially the role of an electrostatic built-in field or a barrier at the FTO/TiO_2 interface has been an issue of great controversy.[1−7] For DSSCs with a liquid electrolyte it seems to be agreed that the electrostatic potential upon illumination changes at the FTO/TiO_2 interface,[8,9] and several models have been presented which were based on (a) a built-in potential that limits the open circuit voltage V_{oc},[1] (b) a built-in potential (smaller than V_{oc}) and thermionic emission over a light-induced Schottky barrier,[5,10] or (c) electron tunneling through a narrow potential barrier.[7,11]

DSSCs show a good performance even though the conducting FTO substrate is in direct contact with the redox electrolyte, due to a low recombination current at the FTO/electrolyte interface. Attempts to reduce this recombination current further were done with a compact TiO_2 layer, which was introduced between the FTO substrate and the mesoporous TiO_2 film to prevent direct contact between the FTO and the electrolyte. While DSSCs with liquid electrolyte give reasonable efficiencies with and without a compact layer, it is crucial for the operation of nanocomposite ETA cells, where the liquid electrolyte is replaced by a solid-state hole conductor. Such devices apparently do not show any significant performance without the compact layer due to a high recombination current from the FTO into the hole conductor.

* To whom correspondence should be addressed. E-mail: sven.ruehle@weizmann.ac.il.

† Weizmann Institute of Science.

‡ Hahn-Meitner-Institut.

§ E-mail: dittrich@hmi.de.

In this work we used photocurrent transient measurements to probe the electric field at porous TiO_2/FTO and compact TiO_2/FTO interfaces, immersed into electrolyte. The transient technique is known as a powerful tool to investigate electron transport in mesoporous TiO_2 films[12,13] and compact, dielectric thin films.[14] An external electrostatic potential and the pH of the electrolyte were varied in the experiments. Current transients of compact TiO_2 layers show the same effect when the potential or the pH value is varied, while mesoporous films respond differently. We discuss the difference in the electrostatic potential distribution for systems with and without compact TiO_2 layer and the implications for solar cell performance.

Experimental Section

Compact and porous TiO_2 films were deposited onto glass substrates covered by conducting FTO (Pilkington TEC 8; sheet resistivity of 8 Ω/square). The compact TiO_2 layers were prepared by spray pyrolysis at a temperature of 450 °C, using a "Camag" spray head (Camag, Muttenz, Switzerland). A spray procedure similar to the one described in ref 15 was applied with a precursor solution containing 200 mM titanium tetra-isopropoxide and 400 mM acetylacetone in ethanol. A film thickness of about 100 nm was obtained. After spray-deposition the samples were left at 450 °C for another 15 min before cooling to room temperature. Porous TiO_2 films were deposited by screen-printing of a paste of TiO_2 nanoparticles, with an average diameter of 25 nm (Degussa P25). The paste was prepared by dissolving the TiO_2 powder in acetic acid (pH 2) and keeping it for several minutes in ultrasound to break P25 aggregates. Carbowax was added to avoid cracks in the films. After drying in air, an interconnected network of TiO_2 nanoparticles was formed by annealing (at 250 °C for 30 min) and subsequent sintering (at 450 °C for 30 min). The thickness of the porous TiO_2 film was ∼5 μm.

The measurements were performed in a homemade electrochemical cell (schematically depicted in Figure 1), which was

10.1021/jp046211y CCC: $30.25
Published on Web 04/22/2005

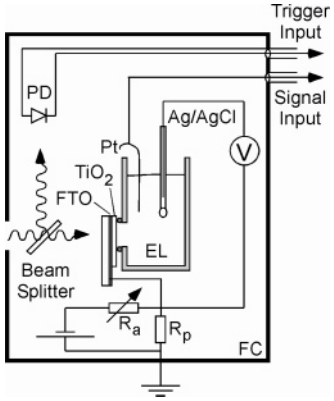

Figure 1. Experimental setup of the screened electrochemical cell for measurements of photocurrent transients.

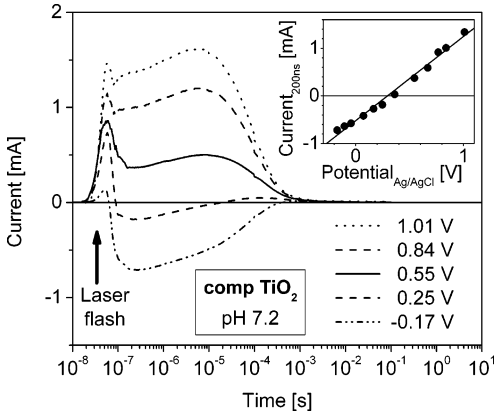

Figure 2. Photocurrent transients of a compact TiO_2 film measured in aqueous LiCl electrolyte (pH 7.2) at different potentials vs Ag/AgCl. The insert gives the potential dependence of the current measured at 200 ns.

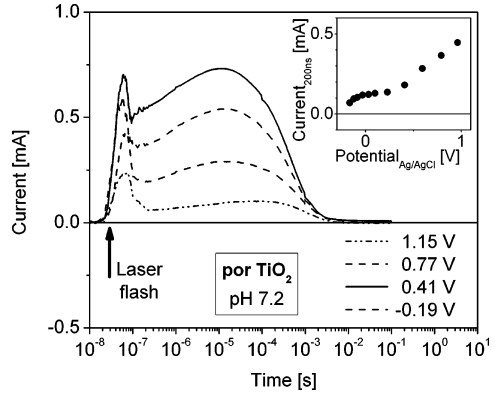

Figure 3. Photocurrent transients of a porous TiO_2 film measured in aqueous LiCl electrolyte (pH 7.2) at different potentials vs Ag/AgCl. The insert gives the potential dependence of the current measured at 200 ns.

electrostatically screened by a Faraday cage (FC). The samples were sealed with an O-ring and grounded for pH-dependent measurements. For potential-dependent measurements, the potential was applied to the FTO contact by a battery, where the voltage was adjusted by a potential divider with a fixed resistor R_p of 50 Ω and variable resistors (R_a). The applied potential was changed between −0.2 and +1.2 V and measured with respect to an Ag/AgCl reference electrode. A Pt counter electrode close to the sample surface was used to measure the photocurrent transients.

Photocurrent measurements were carried out in aqueous NaCl and LiCl electrolytes (EL). For pH-dependent measurements, NaCl was used instead of LiCl to decrease the relative influence of the small Li^+ ions at the metal oxide/electrolyte interface. As a remark, the overall trends were very similar for both NaCl and LiCl electrolytes. The pH of the electrolyte was adjusted between 1 and 12 by adding drops of NaOH or HCl.

The samples were illuminated via the glass substrate to have generation of excess charge carriers in the contact region. Excess charge carriers were generated by pulses of a N_2 laser (wavelength, 337 nm; duration time, 0.5 ns; intensity ∼ 0.1 mJ/pulse; illuminated area ∼ 0.2 cm^2). As a remark, the transmission of the substrate is about 40% and the absorption depth in TiO_2 is about 100 nm at the wavelength of 337 nm. The photocurrent transients were recorded with an oscilloscope (Hewlett-Packard, 54510B), which was externally triggered by a photodiode (PD). The input resistance of the scope was 50 Ω (dc mode), and each transient was averaged 10 times (repetition rate, 1 Hz) to get a stabilized signal.

Results

Potential Dependent Photocurrent Transients. Figure 2 shows photocurrent transients at different potentials, measured on a compact layer. The arrow in the figure marks the laser excitation. The transient current at times below 150 ns is superimposed by an electric noise signal caused by the electric discharge of the laser system during operation, which was not entirely screened by the Faraday cage. A similar signal was observed in reference measurements recorded on bare FTO substrates in contact with electrolyte (not shown). Therefore we do not consider in general the transient current at times shorter than 150 ns for further discussion (Figures 2−5). At longer times, the photocurrent is negative at low and positive at high potentials. The photocurrent decays within about 1 ms. The insert shows the photocurrent at 200 ns (which is shorter than the RC time constant of the system; see below) as a function of the external applied potential. The slope of the linear fit, shown in the insert, corresponds to a resistance of about 0.57 kΩ.

Photocurrent transients measured on a porous TiO_2 film at different potentials are presented in Figure 3. In contrast to the compact TiO_2 film, it was impossible to observe negative photocurrents. The insert of the figure shows the photocurrent at 200 ns as a function of the applied potential, which has a linear regime for applied potentials higher than 0.4 V. Below that the current shows a nonlinear dependence.

pH-Dependent Transient Measurements. Figure 4 shows photocurrent transients, measured on a compact TiO_2 film at different pH values of the electrolyte. The transients are very similar to those measured at different potentials. At the lowest pH value, a negative photocurrent has been observed at 200 ns. The photocurrent increases with increasing pH, similarly to the case of increasing applied potential, as shown before. At 200 ns the photocurrent depends linearly on the pH value (insert of Figure 4) with a slope of ∼0.1 mA/pH.

Photocurrent transients measured on a mesoporous TiO_2 film at different solution pH values are shown in Figure 5. The transient current does not change its sign even at low pH values, which is similar to potential-dependent measurements on porous films. In contrast to potential-dependent measurements, the transients have a different shape and a shift of the transient peak toward longer times is observed when the pH value is increased. The insert of Figure 5 shows a linear dependence between the transient current recorded at 200 ns and the pH value. The slope

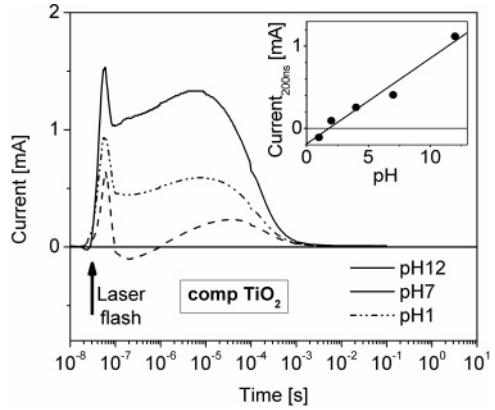

Figure 4. Photocurrent transients of a compact TiO_2 film measured in aqueous NaCl electrolyte for different pH values at zero potential. The insert gives the dependence of the current measured at 200 ns on the pH value.

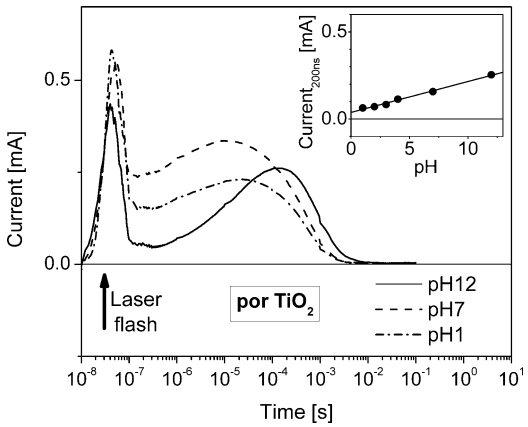

Figure 5. Photocurrent transients of a porous TiO_2 film measured in aqueous NaCl electrolyte for different pH values at zero potential. The insert gives the dependence of the current measured at 200 ns on the pH value.

of 0.02 mV/pH is different from the slope of the pH-dependent measurements on a compact TiO_2 layer.

Discussion

To analyze the electrostatic field at the FTO/TiO_2 interface, we are focusing on the current response at a transient time $t = 200$ ns. A quantitative analysis of the entire transient shape and the location of the maximum are beyond the scope of this paper.

Compact TiO_2/FTO Interface. We attribute the linear dependence of the transient current at $t = 200$ ns as a function of the applied potential difference between the FTO substrate and the electrolyte, together with the change of the current polarity (insert of Figure 2), to a dominant drift current component, $\vec{J}^{d} = q(n\mu_n + p\mu_p)\vec{E}$. The elementary charge is denoted as q, n, and p are the electron and hole densities, while the respective mobilities are given by μ_n and μ_p. Schematic drawings of the compact TiO_2/FTO system at positive and negative applied potential including the electrostatic field ($\vec{E}$) are shown in Figure 6a,b, respectively. The dominant drift current component indicates that most of the laser-induced electron/hole pairs are generated within an electric field from which we derive energy band diagrams, shown in Figure 6c,d. The bottom of the conduction band and the top of the valence band are denoted as E_{CB} and E_{VB}, respectively, and the band diagrams include a band discontinuity at the FTO/TiO_2 interface.[16] This band offset promotes electron transfer to the FTO

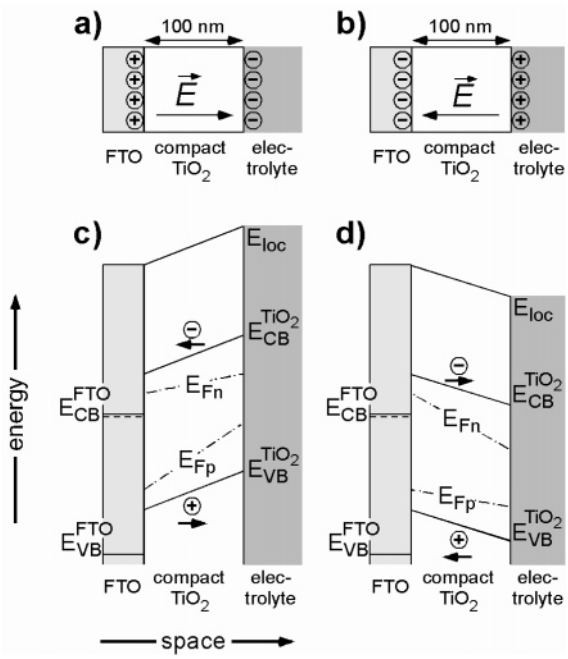

Figure 6. Scheme of the FTO/compact TiO_2/electrolyte system for opposite electrical fields (a, b) and respective band structures, which show the potential distributions in the compact TiO_2 films (c, d). The local vacuum level is denoted by E_{loc}.

substrate and blocks hole transfer. The electron and hole quasi Fermi levels (E_{F_n} and E_{F_p}) are depicted for the system immediately after photoexcitation, and the drift directions of electrons and holes are indicated by arrows underneath the charges. Band bending across the compact TiO_2 layer, as proposed in ref. 17, is neglected,[18] even though some band bending might be superimposed to the depicted band structure, but does not change the direction of the drift current.

Photocurrent transients measured on compact TiO_2 layers as a function of the electrolyte pH show also a linear behavior of the transient current at 200 ns. In oxide semiconductors, the energy levels of the band edges depend on the surface pH due to specific adsorption of OH^- and H^+ ions. The energy bands shift toward the vacuum level with increasing pH by 59 mV/pH, if specific adsorption of other ions from the solution is negligible.[19] The compact nature of the TiO_2 layer prevents interaction of the electrolyte with the FTO/TiO_2 interface such that the band alignment at this interface is defined by the intrinsic TiO_2 and FTO properties, while the energy levels at the liquid interface are defined by the pH value. If we convert the slope of 0.10 mA/pH into a resistivity (using a band shift of 59 mV/pH) we find a value of 0.58 kΩ, which is in excellent agreement with the value of 0.57 kΩ from the potential-dependent measurements. We conclude that an electrostatic field can be introduced into a compact TiO_2 layer with a polarity which is defined by the pH of the electrolyte. The origin of this field is explained in Figure 7. A TiO_2 semiconductor surface in contact with a basic electrolyte at thermal equilibrium (shown by a constant Fermi level E_F) is shown in Figure 7a. The negative excess charge at the TiO_2 surface, due to dominant adsorption of OH^- ions, is charge-compensated by positive charges in the depletion layer (DL). The situation is reversed for a TiO_2 surface in contact with acetic solution (Figure 7b), where the positive excess charge on the TiO_2 surface is compensated by negative charge in the accumulation layer (AL). The pH-dependent change of the accumulation or depletion layer width can be measured as a shift of flat band potential in Mott–Schottky experiments.[20] In our case the investigated compact

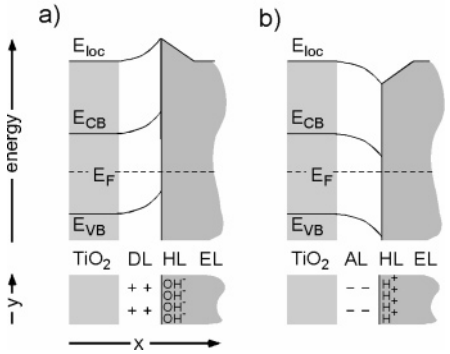

Figure 7. Energy band diagrams at the surface of bulk TiO_2 in contact with basic (a) and acetic electrolyte (b) at thermal equilibrium. The excess charges in the depletion layer (DL), in the accumulation layer (AL), and on the TiO_2 surface are depicted below the band structures. The charges of the Helmholtz (HL) layer are not explicitly shown.

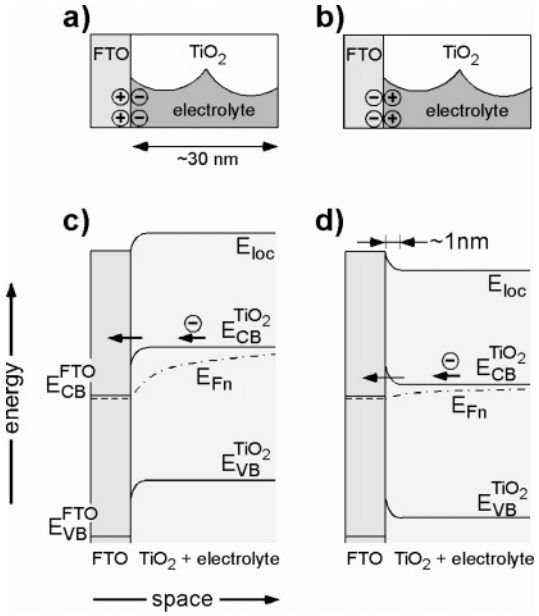

Figure 8. Scheme of the FTO/porous TiO_2/electrolyte system for opposite electrical fields (a, b) and respective potential distributions in the porous TiO_2 films for the first two layers of nanoparticles in contact with the FTO (c, d).

TiO_2 layers were thinner than the required width of a space charge layer so that most of the charge was compensated at the FTO substrate. Thus, band diagrams for pH-dependent measurements are similar to the diagrams depicted in Figure 6.

Porous TiO_2/FTO Interface. Photocurrent transients of the porous TiO_2/FTO electrolyte system do not show any change in the sign of the current response. We interpreted this by an absence of a drift current component and conclude that most of the excess charge carriers are generated in a region which is field-free. In the mesoporous TiO_2 system, the applied electrostatic potential difference between the FTO substrate and the electrolyte drops across a Helmholtz layer at the FTO/electrolyte interface, as shown in Figure 8a,b. The electrostatic potential distribution inside the TiO_2 particles is determined by the potential of the FTO and the electrolyte. Theoretical analysis predicts that the potential in the TiO_2 drops within the first layer of particles in contact with the FTO substrate.[1,10,11,21] Energy band diagrams for the first two layers of TiO_2 particles in contact with the FTO are depicted in Figure 8c,d. They show the sharp electrostatic potential drop at the FTO/TiO_2 interface for positive (Figure 8c) and negative applied potential, where it creates a barrier (Figure 8d). The positive transient current at negative applied potentials indicates that the electrostatic barrier is sufficiently narrow for efficient electron tunneling through it and does not completely block electron transfer into the FTO. Hole transport in the mesoporous system is not considered because holes are much faster injected into the electrolyte than electrons.[13]

We explain the potential dependence of the current transients by a difference in the gradient of E_{Fn}, also shown in Figure 8c,d. The gradient of E_{Fn} at positive applied potential is bigger than at negative applied potential, which results in a stronger current at positive applied potentials and is consistent with the experiments (Figure 3). We interpret our results as direct experimental support for the theoretical predicted electrostatic potential distribution at the porous TiO_2/FTO interface.[1,10,11,21]

Transient measurements on porous TiO_2 samples as a function of the pH value have to be differently interpreted. H^+ and OH^- ions affect the band energy levels of TiO_2 and the FTO in a similar fashion. Therefore it is not expected that the electrostatic field at the FTO/TiO_2 interface is significantly changed as a function of the pH value. We attribute the observed pH dependence to a difference in the trap distribution that affects the effective electron diffusion coefficient in the mesoporous TiO_2.

Impact of the RC Time Constant. The capacitance of the mesoporous TiO_2/FTO system in contact with electrolyte is $\sim 5\ \mu F/cm^2$ and approximately 1 order of magnitude smaller for the compact TiO_2/FTO system.[22] Thus, the RC constant is 50 μs for the mesoporous and 5 μs for the compact systems, which are both significantly bigger than $t = 200$ ns, at which the current signal was analyzed. For $t \ll$ RC the current signal is integrated, which results in a smoothing of the photocurrent transient. It has to be emphasized that the RC constant does not affect the current polarity at $t \ll$ RC,[2] so that our interpretation of the presence and absence of a drift current component remains valid.

Electrostatic Field in DSSCs and ETA Cells. Potential- and pH-dependent transient measurements of the compact TiO_2/FTO system show that most of the charge carriers are generated within an electric field in contrast to the mesoporous TiO_2/FTO system, where most of the carriers are generated outside an $\vec{E}$ field. This means that an electrostatic potential difference drops throughout the entire compact TiO_2 layer in contrast to the mesoporous TiO_2/FTO interface, where it drops on a very small distance. For the operation of DSSCs the spatial extension of the $\vec{E}$ field is of minor importance as long as it promotes electron transfer from the TiO_2 into the FTO substrate. In contrast this field can limit the performance of DSSCs when it creates a barrier for electron transfer at voltages below V_{oc}.[5,11] Electrons have to overcome this barrier by thermionic emission,[5] cross the barrier by hopping via gap states, or tunnel through it.[7,11] DSSCs are known to show a reasonable performance with and without a compact TiO_2 underlayer, and it has been discussed recently[11] that electron tunneling might be the dominant transport mechanism for systems with a narrow electrostatic barrier (e.g., at the mesoporous TiO_2/FTO interface), while thermionic emission and/or hopping are more likely in a system with a spatial extended barrier (compact TiO_2/FTO interface).

Solid-state ETA cells usually consist of a compact TiO_2 layer, and it was not possible until now to reach similar light to electric energy conversion efficiencies compared to DSSCs. Several ETA cell configurations show reasonable short circuit currents and open circuit voltages, but a rather low fill factor.[22,23] Upon solar cell operation the barrier at the compact TiO_2/FTO interface can be higher in ETA cells due to a different work

function of the used solid-state hole conductor. This spatially extended barrier across the compact layer can be reason for the experimentally observed S-shape of the $I-V$ characteristics that leads to the low fill factor and, thus, to a low efficiency. Our results indicate that the performance of ETA cells can be improved when the electrostatic barrier is narrowed down, such that electron tunneling becomes significant.

Conclusions

Photocurrent transient measurements were used to probe the electric field at the interface between the FTO substrate and a compact or porous TiO_2 film immersed in electrolyte. Transients of the FTO/compact TiO_2/electrolyte system as a function of an externally applied potential or at different solution pH show equal behavior, while the situation is more complicated for the FTO/porous TiO_2/electrolyte system. We interpret our results in terms of (i) an electric field that is present throughout the compact layer, while (ii) the electrostatic potential drops on a very narrow region at the nanoparticle/FTO interface. For solar cells this suggests that the electron transport mechanism at the TiO_2/FTO interface is fundamentally different when an electrostatic barrier is present upon cell operation. Electron tunneling is a possible transfer mechanism at the porous TiO_2/FTO interface due to the small barrier width, while thermionic emission or hopping via gap states are more likely processes at the compact TiO_2/FTO interface, due to a larger barrier width. In solid-state DSSCs or in ETA cells, a compact TiO_2 underlayer is required to avoid direct contact between the FTO substrate and the hole conductor. The fundamental difference of the electrostatic potential distribution at porous TiO_2/FTO and compact TiO_2/FTO interfaces has to be considered for a complete theoretical description of DSSCs.

Acknowledgment. S.R. acknowledges the financial support provided by the Minerva Foundation and the European Union's Human Potential Program under Contract HPRN-CT-2000-00141, ETA Solar Cells. The authors thank Prof. A. Zaban and his group for help in sample preparation and Dr. F. Lenzmann for the supply of the compact TiO_2 layers.

References and Notes

(1) Schwarzburg, K.; Willig, F. *J. Phys. Chem. B* **1999**, *103*, 5743.
(2) Schwarzburg, K.; Ernsthofer, R.; Felber, S.; Willig, F. *Coord. Chem. Rev.* **2004**, *248*, 1259.
(3) Bisquert, J. *J. Phys. Chem. B* **2003**, *107*, 13541.
(4) Rau, U.; Kron, G.; Werner, J. H. *J. Phys. Chem. B* **2003**, *107*, 13547.
(5) Kron, G.; Rau, U.; Werner, J. H. *J. Phys. Chem. B* **2003**, *107*, 13258.
(6) Gregg, B. A. *J. Phys. Chem. B* **2003**, *107*, 13540.
(7) Pichot, F.; Gregg, B. A. *J. Phys. Chem. B* **1999**, *104*, 6.
(8) Schlichthörl, G.; Huang, S. Y.; Sprague, J.; Frank, A. J. *J. Phys. Chem. B* **1997**, *101*, 8141.
(9) Boschloo, G. K.; Goossens, A.; Schoonman, J. *J. Electroanal. Chem.* **1997**, *428*, 25.
(10) Ferber, J.; Luther, J. *J. Phys. Chem. B* **2000**, *105*, 4895.
(11) Rühle, S.; Cahen, D. *J. Phys. Chem. B* **2004**, *108*, 17946.
(12) Nelson, J.; Haque, S. A.; Klug, D. R.; Durrant, J. R. *Phys. Rev. B* **2001**, *63*, 205321.
(13) Solbrand, A.; Södergren, S.; Lindström, H.; Rensmo, H.; Hagfeldt, A.; Lindquist, S.-E. *J. Phys. Chem. B* **1997**, *101*, 2514.
(14) Scher, H.; Montroll, E. W. *Phys. Rev. B* **1975**, *12*, 2455.
(15) Kavan, L.; Grätzel, M. *Electrochim.* Acta **1995**, *40*, 643.
(16) Cahen, D.; Hodes, G.; Grätzel, M.; Guillemoles, J. F.; Riess, I. *J. Phys. Chem. B* **2000**, *104*, 2053.
(17) Cameron, P. J.; Peter, L. M. *J. Phys. Chem. B* **2003**, *107*, 14394.
(18) In contrast to ref 17 we include a bigger CB discontinuity at the FTO/TiO_2 interface; e.g. for a CB discontinuity of 0.6 eV and a trap density of 10^{20} cm^{-3}, located 0.3 eV below the TiO_2 CB edge, we calculate a band bending of 1 meV. Thus we neglect band bending and draw the bands as straight lines.
(19) Gerischer, H. *Electrochim. Acta* **1989**, *34*, 1005.
(20) Watson, D. F.; Marton, A.; Stux, A. M.; Meyer, G. J. *J. Phys. Chem. B* **2003**, *107*, 10971.
(21) Bisquert, J.; Garcia-Belmonte, G.; Fabregat-Santiago, F. *J. Solid State Electrochem.* **1999**, *3*, 337.
(22) Belaidi, A.; Bayón, R.; Dloczik, L.; Ernst, K.; Lux-Steiner, M.-C.; Könenkamp, R. *Thin Solid Films* **2003**, *431*, 488.
(23) Ernst, K.; Engelhardt, R.; Ellmer, K.; Kelch, C.; Muffler, H.-J.; Lux-Steiner, M.-C.; Könenkamp, R. *Thin Solid Films* **2001**, *387*, 26.